

GT-2002-30053

OBSERVATIONS OF FLAME BEHAVIOR IN A LABORATORY-SCALE PRE-MIXED NATURAL GAS/AIR GAS TURBINE COMBUSTOR FROM LDA VELOCITY MEASUREMENTS

Paul O. Hedman, Robert L. Murray, and Thomas H. Fletcher
Department of Chemical Engineering, Brigham Young University, Provo, Utah, USA 84602

ABSTRACT

The objective of this study was to obtain simultaneous axial/radial and axial/tangential velocity measurements in a laboratory-scale, gas-turbine combustor (LSGTC) with a pre-mixed, swirl-stabilized, natural gas flame. Velocity measurements were obtained at each of four operating conditions (high swirl and medium swirl at fuel equivalence ratios of 0.80 and 0.65). Example results of mean and standard deviation axial, radial, and tangential velocities are included in this paper for the high swirl (HS), $\phi = 0.80$ case (most stable flame) and the medium swirl (MS), $\phi = 0.65$ case (least stable case). Additionally, example probability density distributions (PDF) for the axial velocity at the 80 mm axial location are presented for the same two cases. The velocity and PDF data show greater stability for the HS cases than the MS cases. Sizes and strengths of recirculation zones are determined, showing a larger degree of central recirculation in the HS cases, which is thought to be responsible for enhanced stability in this premixed system.

INTRODUCTION

This study was part of a series of laser-diagnostic experiments performed on a common combustion apparatus. Companion studies were performed to make planar laser induced fluorescence (PLIF) images of OH [1] and to measure gas temperatures and concentrations using coherent anti-Stokes Raman spectroscopy (CARS) [2-3]. These data were obtained principally for evaluation of comprehensive gas turbine combustion models [4-7]. The work presented here is the result of two-component laser Doppler anemometry (LDA) measurements of instantaneous velocities obtained in a laboratory-scale, gas-turbine combustor (LSGTC) with a pre-mixed, swirl-stabilized, natural gas flame. The LSGTC was operated at two swirl conditions and two fuel equivalence ratios (0.80 and 0.65) at atmospheric pressure. This paper reports on the instantaneous, mean, and probability density functions (PDF's) of all three components of velocity in this combustor.

Past experience at BYU/ACERC has shown that the modeling of combustion behavior is more accurate and proceeds more rapidly when coupled with pertinent, foundational

experimental research. The LSGTC simulates many of the key combustor characteristics of commercial gas turbines [8], and provides a realistic flame where model predictions and in situ measurements can be compared. Use of advanced optical diagnostics has permitted near-instantaneous, non-intrusive LDA measurements of velocity, CARS measurements of temperature, and PLIF images of flame shape. These experimental measurements provide insight into the physical processes that govern the combustion processes, provide direction to the modeling of the combustion process, and have also provided a database suitable for model sub-code evaluation and verification.

The objective of this part of the experimental program was to obtain approximately 4000 instantaneous measurements at each diagnostic location in the combustor (126 locations for the axial/radial sets, and 196 locations for the axial/tangential sets). The instantaneous measurements were analyzed to obtain mean and standard deviation velocities at each location. Software interpolation of the specific mean and/or standard deviation values has allowed creation of iso-contour plots (or false color maps) of the mean and standard deviation velocities in the flame zone. Examples plots are included in this paper for the HS $\phi = 0.80$ case (most stable flame) and the MS $\phi = 0.65$ case (least stable flame). Additionally, probability density functions (PDF) have been determined from the 4000 instantaneous measurements at selected locations in the combustor. Example axial velocity PDFs at the 80 mm axial location are presented for the same two cases. The complete set of results for all four test cases is reported by Murray [15].

NOMENCLATURE

CRZ	central recirculation zone
h	height
HS	high swirl condition
lpm	liters per minute
MS	medium swirl condition
PDF	probability density function
Q	flow rate
r	radius
SN	swirl number
SRZ	side recirculation zone
w	width

equivalence ratio

Subscripts

c	central (referring to central recirculation zone)
s	side (referring to side recirculation zone)
u	axial velocity
v	radial velocity
w	tangential velocity
x	horizontal distance from centerline
z	vertical distance from burner surface

COMBUSTOR TEST FACILITY

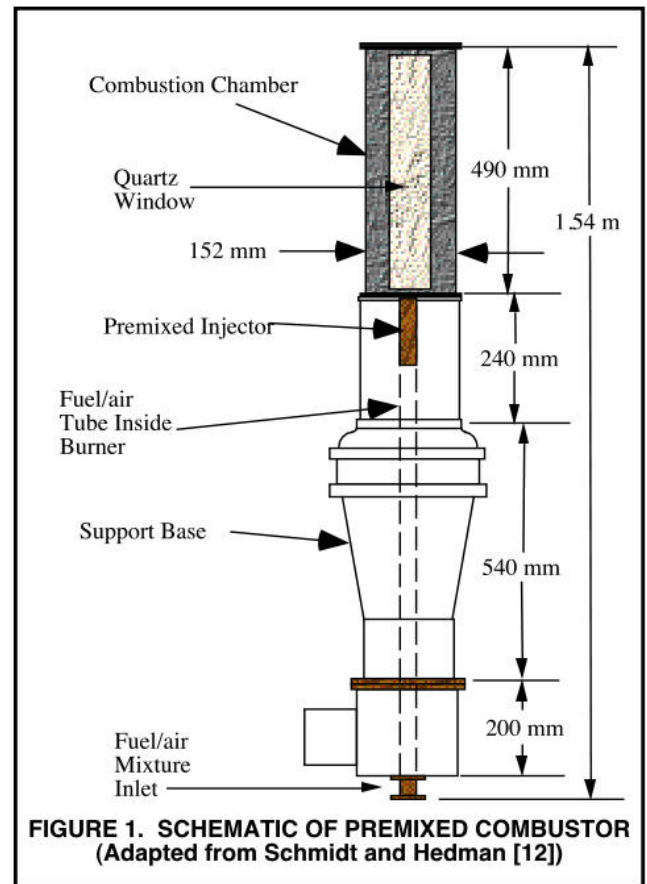
The combustion facility used for this study is the same as that used by [9-11]. Schmidt and Hedman [12] incorporated a premixed injector and used the burner to make CARS temperature and LDA velocity measurements on a premixed propane/air flame. The facility was further modified for this study to allow investigation of a premixed natural gas/air flame. This new premixed natural gas/air combustor has been designated the ATS Burner (developed for the US/DOE Advanced Turbine Systems program).

The actual combustion chamber, illustrated in Figure 1, was designed to reproduce the characteristics found in a modern annular combustor [8]. The combustor, which was provided to BYU by Wright Laboratory, Wright-Patterson Air Force Base [13], consists of a four-sided chamber with metal fillets in the corners to more nearly simulate an axisymmetric combustor while maintaining adequate optical access. Each of the four walls can be either a metal plate or a quartz window, depending on the optical access required. The premixed swirl injector, illustrated in Figure 2, is located in the center of the combustion chamber base. The injector consists of a stainless steel tube with a honeycombed brass insert. The brass insert serves to smooth the flow as well as provide a flame arrestor in case of flashback in the premixed fuel air mixture. Inserts are installed in the injector to provide different magnitudes of swirl to the inlet flow. The swirler inserts are placed above the brass honeycomb and secured by a threaded post that anchors the swirler to the brass honeycomb. A cap with an 18-mm hole in the center and beveled walls is placed on the top of the steel tube to coalesce the swirling flow at the injector exit. This cap was needed in order to make the burner operate successfully.

Figure 2 also shows a schematic of the two swirl inserts used in this study. The swirl inserts are labeled high swirl (HS) and medium swirl (MS) to coincide with the 60 and 45-degree slot angles. The swirl number (SN) indicated in Figure 2 is a non-dimensional number that ratios the axial flux of tangential momentum to the axial flux of axial momentum times the equivalent nozzle radius [14]. A swirl number close to zero ($SN \ll 1$) means the axial momentum is very large compared to the tangential momentum, whereas a very large swirl number ($SN \gg 1$) indicates that the axial momentum is small compared to the tangential momentum.

Fuel flow to the burner was measured with a variable area flow meter and is reported in standard liters per minute, or slpm, referenced to 1 atm (101 kPa) and 70°F (21.1°C). The airflow to the burner was controlled by varying the pressure upstream of a choked flow nozzle. The diameter of the choked flow nozzle used for this study was 3.77 mm, and provided airflow rates from 250 to 1000 slpm, depending on upstream pressure. Uniform mixing of gaseous fuel and air was assured by: (a) the length of the tube from the mixing point to the burner; (b) by a jet mixer in the feed system; and by (c) a

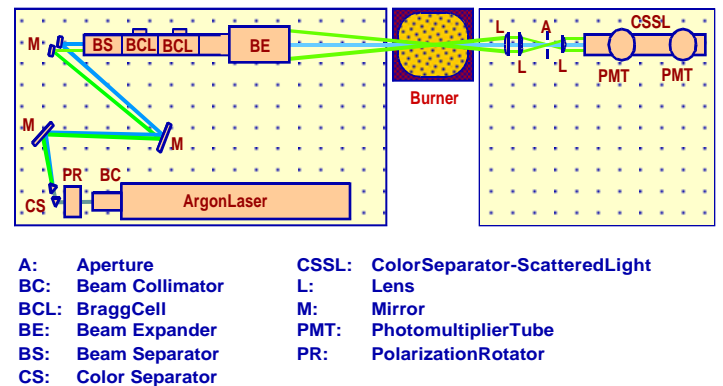
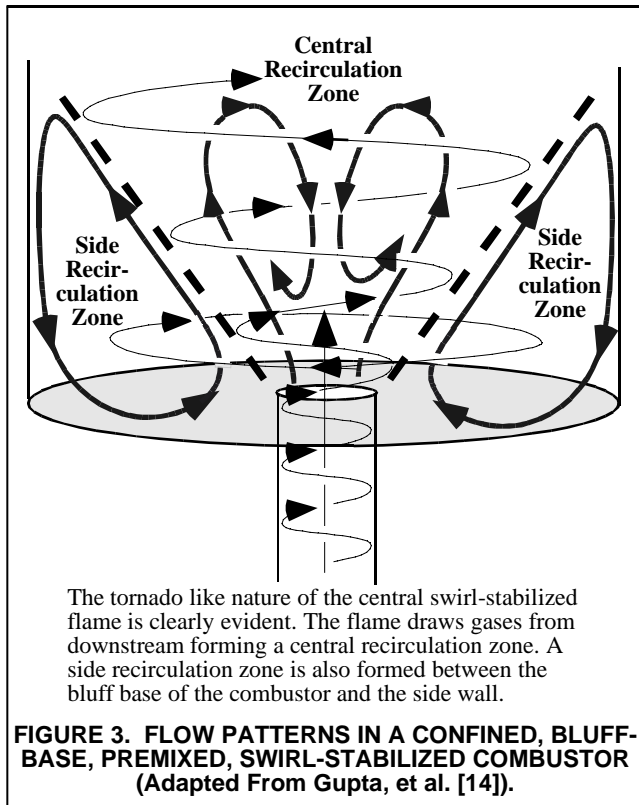
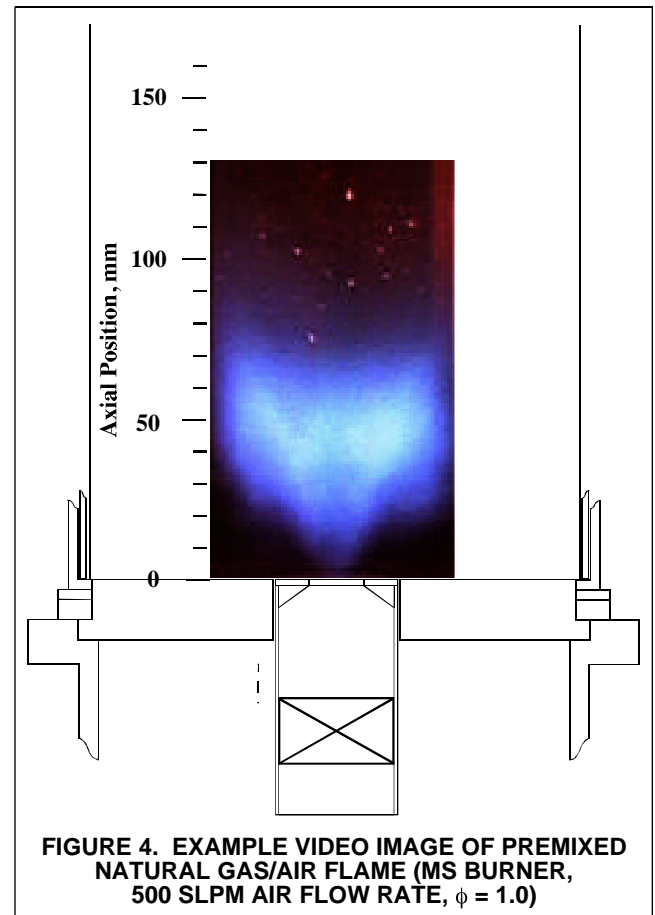
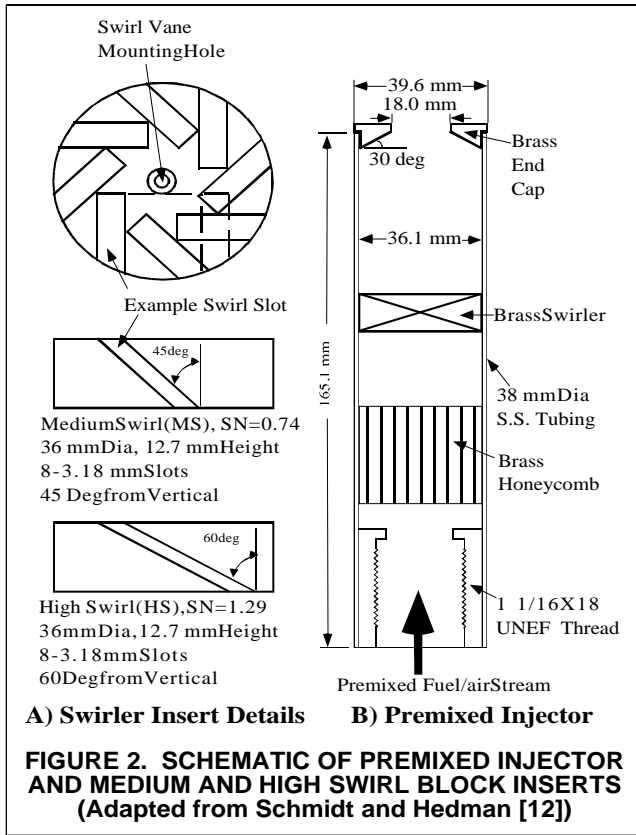
honeycomb flame arrestor. The airflow rate for the four test conditions used in this study was 500 slpm.



VISUAL FLAME IMAGE CHARACTERIZATION

Figure 3 presents a schematic drawing of the flow patterns present in the swirl-stabilized flame. The swirling flow creates a funnel or tornado-like vortex flow centered on the injector exit. A central recirculation zone and a side recirculation zone accompany the tornado-like flow. Both recirculation zones have been found to influence flame stability. Depending on swirl number and fuel equivalence ratio, one or the other of the recirculation zones may dominate the flame stability [15].

Wide variations in flame shape have been observed in the ATS Burner for different combinations of swirl number and fuel equivalence ratio. These structures were studied both visually, through photographic and video recordings, and with the PLIF images obtained in this study. Such observations have yielded insight into the location of the flame front, variation of flame structure with operating conditions and the presence and strength of the recirculation zones. These flame shapes are primarily a result of the effect of the swirl intensity and fuel equivalence ratio on the flow field, with the magnitude of the airflow rate being of secondary importance. The equivalence ratio was varied by changing the fuel flow rate while maintaining a constant 500-slp air flow rate. The changes in flame shape were observed using the point of attachment, the location of the flame front, the structure of the vortex, and the visible intensity of the flame.



An example of a visual image of the flame structure is presented in Figure 4 for a stoichiometric ($\phi = 1.0$), medium swirl case. The $\phi = 1.0$ image was included in the paper because this image was brighter, more visual, and reproduced better. The images at four test conditions (not included herein) are similar and show a small but significant effect of swirl number and fuel equivalence ratio even over the fairly narrow range of operating conditions (HS and MS injectors, and $\phi = 0.80$ and 0.65). Operation at wider limits in fuel equivalence ratio demonstrated wide variations in the observed flame structures. Nevertheless, the images from the four specified test conditions show significant variations with swirl number and ϕ . Operation at $\phi = 0.80$ produced the most stable flames. The flame with the high swirl injector was more coalesced and closer to the injector than with the medium swirl injector. At $\phi = 0.65$, the flame was near the lean flammability limit, and was quite unstable for both swirl injectors. With the medium swirl injector, the flame would oscillate between two different flame structures, one that was more or less attached to the vortex funnel, and one that was lifted well above the vortex funnel. The MS case at $\phi = 0.65$ was at the very edge of the lean flammability limit, and on occasion would actually extinguish.

MEAN GAS VELOCITY MEASUREMENTS

Webb and Hedman [16] set up an LDA system at Brigham Young University (BYU) with a single color beam configured in backscatter mode. They used this system to make velocity measurements in an isothermal flow that was designed to simulate the characteristics of a coal-fired reactor. Following Webb's study, Jones [17] adapted the one color, backscatter, LDA setup to make velocity measurements in a simulated entrained flow reactor. These two studies provided the initial starting point for the current LDA system. Lindsay et al. [18] incorporated additional components into the one-color, backscatter system to form a two-color instrument capable of measuring two component velocities simultaneously. He used the two-color, backscatter LDA system to make velocity measurements in a simulated coal gasifier with swirl. Schmidt and Hedman [12] used a two-color LDA system that was modified to a forward scatter mode. The modified system provided sample rates that were an order of magnitude greater than sample rates taken using a backscatter setup. Following the modification, the instrument was installed on the current LSGTC test stand.

The LDA setup used in this study (Figure 5) is similar to the setup used by Schmidt and Hedman [12]. The argon-ion laser was operated in multi-line mode which lased at several frequencies simultaneously. The multifrequency laser beam was passed through a collimator to reduce beam divergence, and then polarized. A color separator and mirrors were used to select the two strongest wavelengths, 488 nm wavelength (blue) and 514.5 nm wavelength (green). The green beam was split into two beams in the horizontal plane, and the blue beam was split into two beams in the vertical plane. One of the green and one of the blue beams were passed through separate Bragg cells which allowed negative velocities to be obtained. The four beams were passed through a beam expander and focused into two superimposed elliptical probe volumes with major axes of about 2.3 mm and minor axes of about 0.13 mm. The focal length of the transmitting lens was 762 mm with the beams intersecting at a half angle of 3.1° , and the diameter of the laser beam at the lens face was approximately 4 mm. This two-color, four-beam LDA configuration formed a probe volume

with two fringe patterns at right angles to each other, with a blue fringe spacing of $4.44 \mu\text{m}$ and a green fringe spacing of $4.68 \mu\text{m}$.

The air flow was seeded using hollow aluminum oxide microspheres with an average particle diameter of about $6 \mu\text{m}$. The aerodynamic diameter of these particles should follow all of the gas flow patterns, even in the recirculation zones. The seeding of the air flow occurred prior to the fuel addition point and well before the fuel injector. A particle traversing the probe volume produced two Doppler signals. The fringes of the blue beams gave Doppler signals for the axial velocity component and the fringes of the green beams gave the Doppler signals that corresponded to either the radial or tangential velocity component. Sample rates ranged from 400 counts per second to 10,000 counts per second, depending on where the probe volume was positioned in the flame. Sample rates were significantly lower in the high temperature regions of the flame. The Doppler signals were collected in two different photomultiplier tubes (PMT). Each PMT was connected to a signal processor [19] for filtering and validation. Valid velocity signals were then recorded and stored by computer using a Direct Memory Access (DMA) digital I/O card from TSI and a data acquisition program [20] also developed by TSI.

Figures 6 and 7 provide example axial, radial, and tangential iso-velocity contour plots for the HS $\phi = 0.80$ and the MS $\phi = 0.65$ cases, respectively. The results for the other two cases are reported by Murray [15]. These velocity data provide insights into the recirculation patterns involved in this combustor (see the Discussion section).

FLUCTUATING GAS VELOCITY MEASUREMENTS

The analysis of the approximately 4000 instantaneous velocities obtained at each measurement location in the flame zone allows statistical investigation into the turbulent character of the flame to be made. Example standard deviations for the axial, radial, and tangential velocities were calculated at each location in the combustion chamber and iso-velocity contour plots are shown in Figures 8 and 9 for the HS $\phi = 0.80$ and MS $\phi = 0.65$ cases respectively. Maximum and minimum standard deviation velocities are also included.

Comparison of the standard deviation velocity maps with the corresponding mean velocity maps (Figures 6 and 7) show that the highest standard deviation axial, radial, and tangential velocities occur in the positive velocity flow channel where the fastest positive mean axial, radial, and tangential velocities occur. In addition, the lowest standard deviation velocities occurred in the upper region of the combustion chamber and in the side recirculation zone (SRZ). Lower mean velocities were present in these areas.

Past studies have suggested that a large standard deviation correlated with high turbulence regions [11, 12]. In this study, the largest standard deviations occurred in the same location as the largest mean velocity measurements.

Probability distribution functions (PDFs) have been used to describe the flow characteristics and to confirm the accuracy of the data. Figures 10 and 11 show examples of axial velocity PDFs at an axial position of 80 mm and radial positions from near the centerline to about a 40 mm radial location for the HS $\phi = 0.80$ and MS $\phi = 0.65$ cases. Additional PDF results are included in the thesis by Murray [15]. Labeled on the PDF are: the axial position, radial position, mean axial velocity, and standard deviation. Generally, the PDFs have a near Gaussian distribution in an identifiable flow zone. However, the PDFs

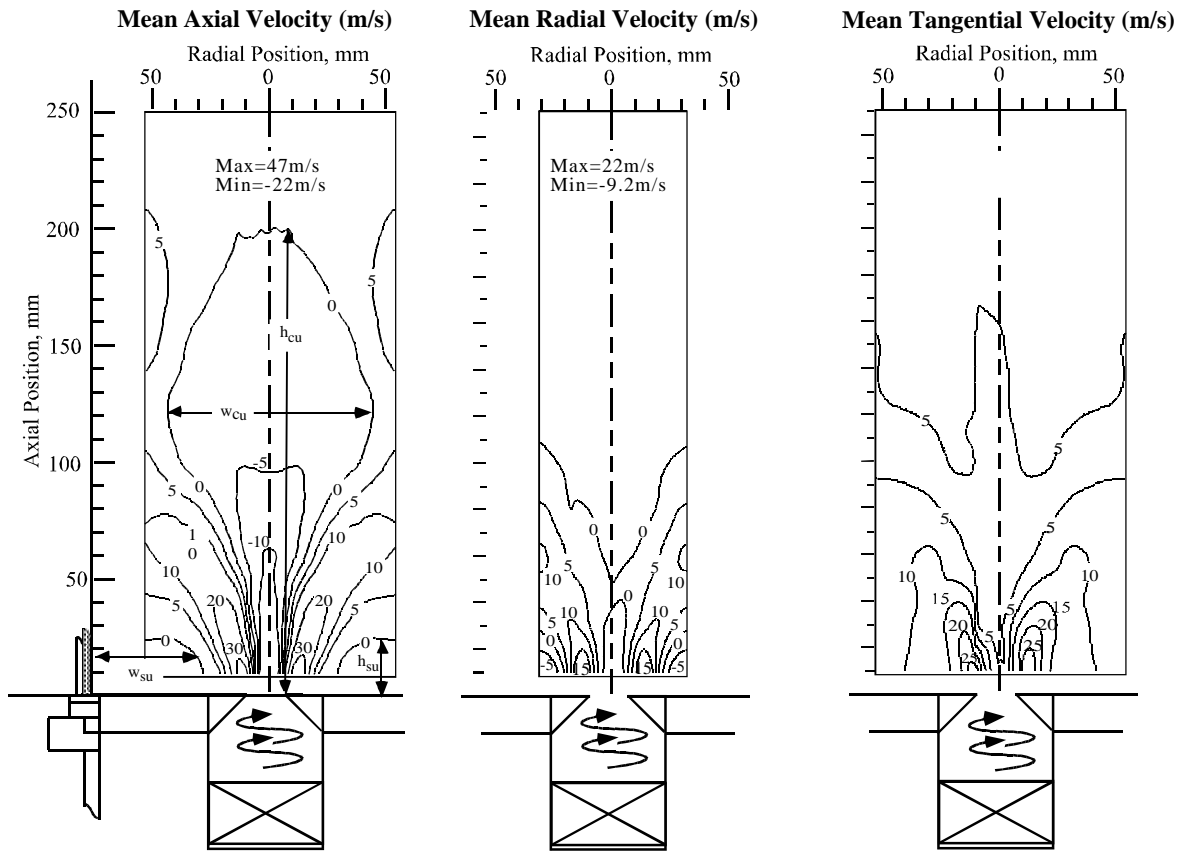


FIGURE 6. ISO-CONTOUR MAPS OF MEAN AXIAL, RADIAL, AND TANGENTIAL VELOCITY, $HS_r = 0.80$

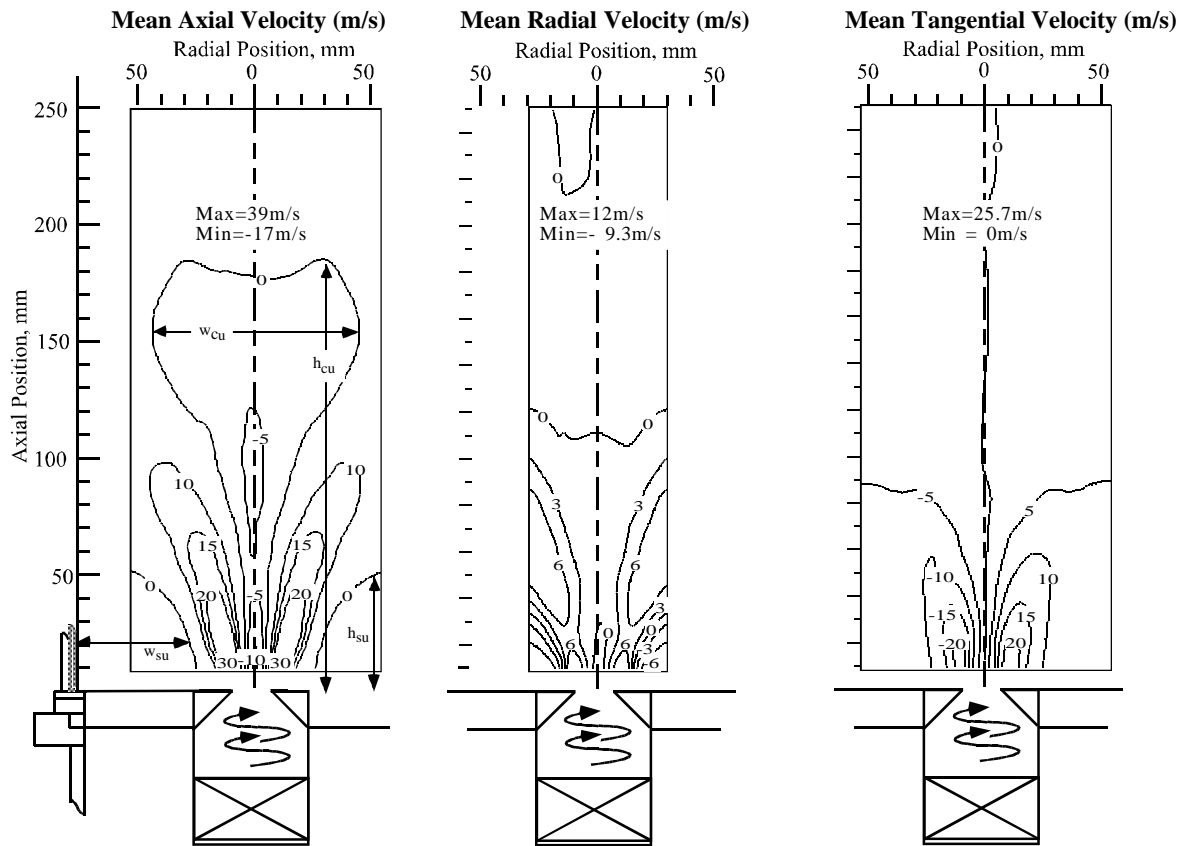


FIGURE 7. ISO-CONTOUR MAPS OF MEAN AXIAL, RADIAL, AND TANGENTIAL VELOCITY, $MS_r = 0.65$

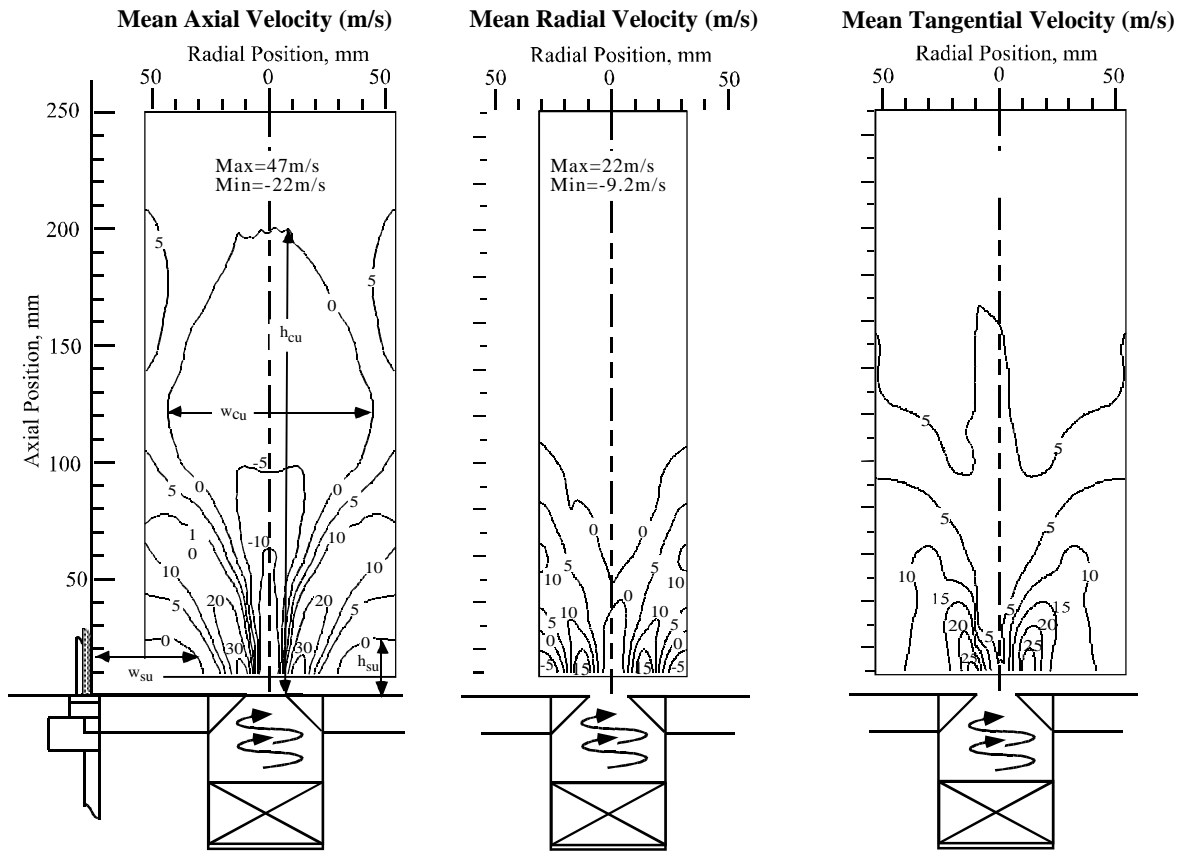


FIGURE 6. ISO-CONTOUR MAPS OF MEAN AXIAL, RADIAL, AND TANGENTIAL VELOCITY, $HS_r = 0.80$

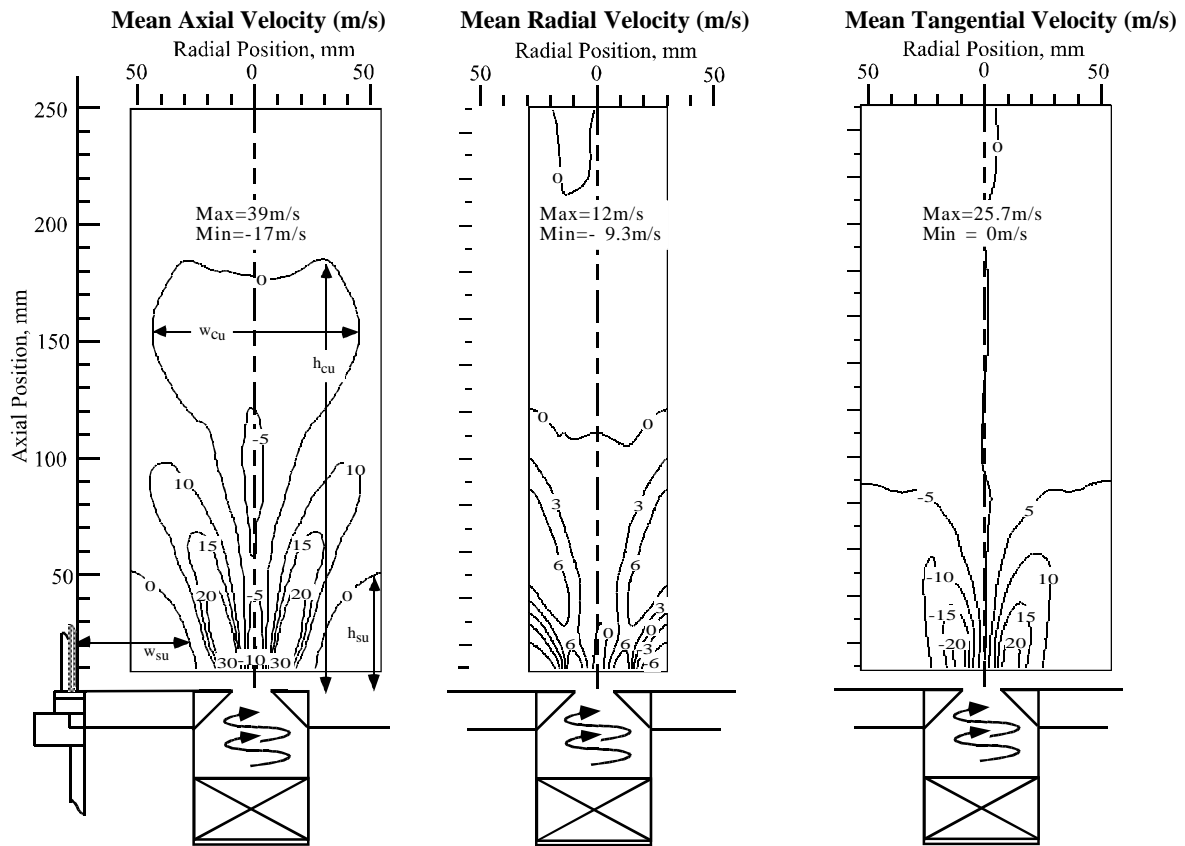


FIGURE 7. ISO-CONTOUR MAPS OF MEAN AXIAL, RADIAL, AND TANGENTIAL VELOCITY, $MS_r = 0.65$

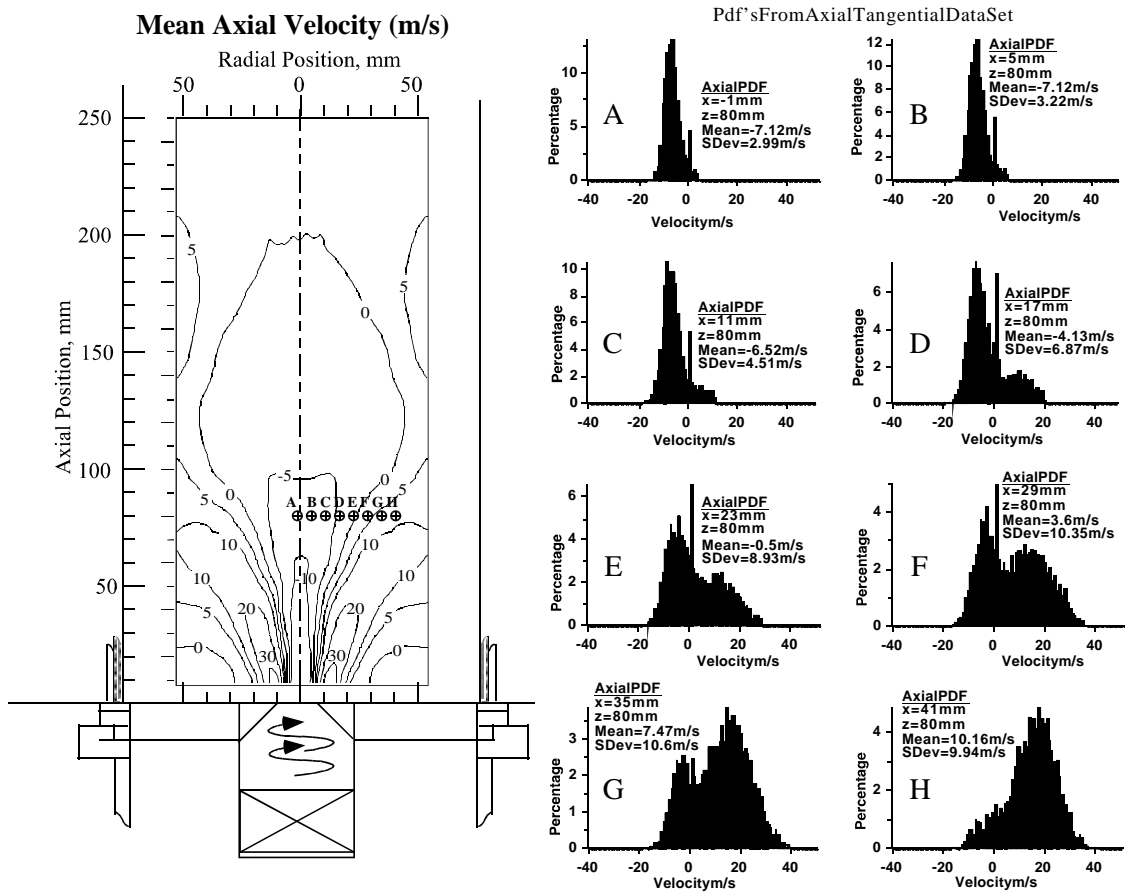


FIGURE 10. MEAN AXIAL VELOCITY CONTOUR MAP AND EXAMPLE AXIAL VELOCITY PDFS, $HS = 0.80$

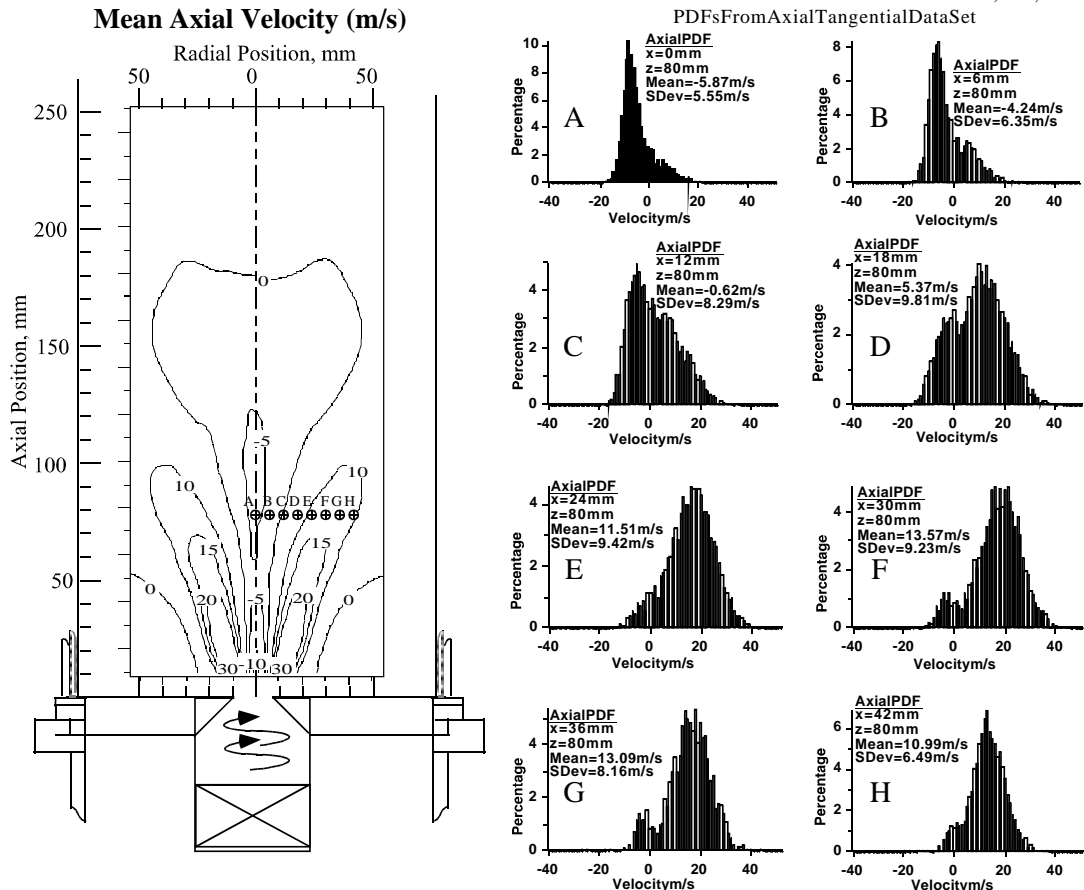


FIGURE 11. MEAN AXIAL VELOCITY CONTOUR MAP AND EXAMPLE AXIAL VELOCITY PDF'S, $MS = 0.65$

had a bimodal distribution when gas velocities were measured across a shear layer between two different identifiable flow zones in the combustor. Typically, this can be seen at a position near the zero velocity contour, and hence the measurements have velocity components from both sides of the zero velocity boundary.

In Figure 10, starting at a radial position of -1 mm, the PDF has a basic Gaussian profile with a slightly increased gradient in the positive velocity region. As measurements move to a radial position of 11 mm, the PDF became less Gaussian with the positive velocity region of the PDF increasing in size, the negative region decreasing in size, and the standard deviation increasing. At 17 mm, the positive velocity region of the PDF has increased significantly. At radial positions of 23 and 29 mm, the positive velocity region of the PDF continues to increase, the mean axial velocity becomes positive overall, the standard deviation continues to increase, and the bimodal peaks are about equal in size and shape. It should be noted that these two positions, (23 mm and 29 mm) straddle the zero axial velocity contour, and hence have velocity components from both sides of the zero velocity boundary. At a radial position of 35 mm, the bimodal distribution continues to be prominent, the positive region of the PDF increases, the positive mean axial velocity increases in magnitude, and the standard deviation remains fairly constant. At a radial position of 41 mm, the negative velocity region of the PDF has nearly disappeared, the mean positive velocity dominates the distribution, and the standard deviation has decreased slightly. Similar observations regarding the changes in PDF distributions as one moves from near centerline past the zero axial velocity contour can be seen in Figure 11 for the $MS = 0.65$ case.

The PDFs observations support the conclusion of strong shear layers in the combustion chamber. Bimodal distributions across the shear layer (zero axial velocity contour) were typically found from an axial position of 60 mm to an axial position of 100 mm. Below an axial position of 60 mm bimodal distributions were sometimes seen, but the spacing between measurements was too great to get a good progression of PDFs. At axial positions above 125 mm, the measured velocities across the shear layer were not high enough to demonstrate the bimodal distributions in the PDFs. Instead, the PDF usually represented a near Gaussian distribution with the peak of the distribution being at or near the axial centerline.

DISCUSSION

Recirculation zones play a major role in stabilizing a turbulent, premixed natural gas combustor. In this study, it was assumed that gas moving down into the ignition zone and radially towards the axial centerline improved the stability of the flame. In other words, the incoming premixed fuel and air needed a source of heat and/or radicals from the recirculated products to stabilize. The intensity of the recirculation zones was based on how well the recirculation zones moved hot gases to the middle of the combustion chamber and down into the ignition zone. Examination of the zero axial velocity and zero radial velocity contours helps define recirculation regions. Zero velocity contours for both the axial and radial velocity maps are shown in both Figures 6 and 7. The sizes of the recirculation zones are directly related to the heights and widths of the zero velocity contours. For convenience, a set of dimensions is defined in Figures 6 and 7. The maximum height of the zero axial velocity contour, measured from the combustor base plate is labeled h_{cu} for the central recirculation zone (CRZ) and h_{su} for

the side recirculation zone (SRZ). The maximum horizontal distance between the zero axial velocity contours for the CRZ is the width of the axial flow channel (w_{cu}), with a similar value (w_{su}) for the SRZ. Murray [15] has used the heights and widths to quantitatively investigate the effect of flow recirculation on flame stability. Only a brief summary of these observations is included in this paper.

The predominant flow path of gases entering the combustion chamber is away from the centerline. A portion of the gases is then recirculated back down the centerline towards the combustor base plate, while the remainder of the gas exits the chamber. This is illustrated in Figure 3. A positive axial velocity flow channel exists between the chamber wall and the zero axial velocity contour. A corresponding negative axial velocity flow channel is seen within the zero axial velocity contour in the CRZ. The CRZ can be divided into two regions. An upper region where products are being feed downward, and a lower region occupied by the visible flame..

Characteristics of the CRZ. The zero axial and radial velocity contours found in the center of the iso-velocity contour plots were used to characterize the CRZ. Three regions of the CRZ were characterized: 1) the maximum upper CRZ boundary (maximum h_{cu}); 2) the negative axial velocity flow channel; and 3) zero radial velocity boundaries. The axial positions of the maximum upper CRZ boundaries are given in Table 1. All of the cases had upper/lower CRZ boundaries at axial positions between 80 mm and 100 mm. Variations in the value of h_{cu} are also reported in Table 1. The value of h_{cu} was greatest for the $MS = 0.80$ case (230 mm). This was 25 mm higher than the value of h_{cu} for the $HS = 0.80$ case. The HS and $MS = 0.65$ cases had the same h_{cu} of 190 mm.

TABLE 1. Characteristics of the Central Recirculation Zone (CRZ)

Measurements	MS =0.65	HS 0.65	MS 0.80	HS 0.80
h_{cu} (mm)	190	190	230	205
w_{cu} (mm)				
• At 50 mm	16	22	20	24
• At 80 mm	24	44	30	48
• At 100 mm	40	60	40	80
• At 125 mm	64	78	90	96
• At 150 mm	92	116	80	80
Axial position of Max.				
w_{cu}	155	150	150	125
Maximum w_{cu}	94	116	80	96
w_{cu} : (mm)				
• At 50 mm	*	22	16	18
• At 80 mm	*	40	16	40
• At 100 mm	*	54	24	52
• At 125 mm	*	>60	*	>60
* Not observed				

The lower boundary of the CRZ was not measured because the lower CRZ extended below the level of the laser access (10 mm). However, in the $HS = 0.80$ case, gases in the lower CRZ were visually identified as flowing into the injector below the base plate of the combustion chamber. This was not unusual for the HS cases.

In premixed flows, recirculation of hot gases containing reactive intermediates is important for flame stabilization. Recirculated gases flowing in the negative axial direction may either be re-entrained before reaching the ignition flame zone (i.e., in an upper part of the CRZ), or else may penetrate into a lower part of the CRZ and hence interact directly with the

flame. The magnitude of flow rates in the CRZ are dependent on the width of the CRZ (w_{cu}) and the magnitude of the negative axial velocities.

The widths of the CRZ (w_{cu}) and the value of w_{cv} (the distance between the zero radial velocity contours) for the different cases are listed in Table 1 for different axial positions in the combustion chamber. Increasing the swirl for a given fuel equivalence ratio had the effect of increasing w_{cu} and w_{cv} , especially at heights of 100 mm or lower.

The wider CRZ dimensions in the HS cases allowed more gas to flow down through the combustion chamber and directed more of the gas to the axial centerline, since maximum negative velocities were about the same in all cases. This wider CRZ in the HS combustion helped flame stability and permitted burner operation at lower equivalence ratios.

Characteristics of the SRZ. The zero axial and radial velocity contours found to the side of the central zero velocity contour were used to characterize the SRZ. The strength of each SRZ was characterized by the following: 1) the height of the zero axial velocity boundary (h_{su}); 2) the width of the zero axial velocity flow channel (w_{su}); 3) the height of the negative radial velocity flow channel (h_{sv}); and 4) the maximum negative velocities in the SRZ. The variables h_{su} , w_{su} , and h_{sv} , and maximum negative velocities are provided in Table 2.

TABLE 2. Characteristics of the Side Recirculation Zone (SRZ)

Measurements	MS =0.65	HS 0.65	MS 0.80	HS 0.80
h_{su} (in mm)	45	38	55	18
Ignition Zone Boundary (in mm)	50	50	40	40
w_{su} at Axial Position of 10 mm (in mm)	23	19	56	11
Maximum Negative Axial Velocity (m/s)	-3.1	-1.4	-3.8	-0.9
h_{sv} (in mm)	32	32	40	29
Maximum Negative Radial Velocity (m/s)	-9.3	-8	-8.4	-9.2

The height of the SRZ (h_{su}) affects flame stability, since the SRZ brings hot gases down to the ignition zone. If h_{su} is too low, only cold unreacted gas will be recirculated and hence the SRZ will not affect flame stability. The MS 0.80 case was the only case where h_{su} was high enough to extend into the flame zone. The MS 0.80 case had a h_{su} of 55 mm. For all other cases, h_{su} was too low to extend up into the flame zone.

The MS cases had a wider value of w_{su} than the HS cases. At an axial position of 10 mm, the value of w_{su} for the MS = 0.80 case was five times wider than the w_{su} for HS = 0.80 case. The value of w_{su} for the MS = 0.65 case was also wider than the w_{su} for the HS = 0.65 case.

The maximum height of h_{sv} could not be obtained for the SRZ because optical measurements were not possible beyond a radial position of 30 mm. However, the value of h_{sv} was characterized by the zero radial velocity contour at a radial position of 30 mm. The h_{sv} for the MS = 0.80 was more than 1.3 times higher than h_{sv} of the HS = 0.80 case. The h_{sv} for the MS = 0.65 was the same as the HS = 0.65 case.

The maximum axial velocity found in the SRZ was almost four times faster for the MS = 0.80 case when compared with the HS = 0.80 case. The axial velocity found in the SRZ was a little over two times faster for the MS = 0.65 case

when compared with the HS = 0.65 case. Maximum negative radial velocities were similar.

In order to characterize the recirculation zones better, the gas flow rates of the recirculation zones at specific axial positions in the combustion chamber were calculated (see Murray [15] for details). Volumetric flow rates were calculated in two regions of the combustion chamber. For this study, the negative flow rate moving through CRZ was labeled Q_c , and the negative flow rate moving through the SRZ was labeled Q_s . The volumetric flow rates were calculated by integrating an axial velocity profile $u(r)$ as a function of the radius across the CRZ. It was assumed that the gas flow in the combustion chamber was axi-symmetric and therefore the axial velocity profile was not a function of the angular position. A comparison is given below between the flow rates at different heights in the combustion chamber. A better comparison between cases could have been made with mass flow rates instead of volumetric flow rates. However, gas densities cannot be estimated without accurate temperature and species concentration data.

The CRZ flow rates (Q_c) are summarized in Table 3. The conclusions drawn are: 1) the MS cases had a higher Q_c at an axial position of 120 mm to 150 mm than observed in the corresponding HS cases; 2) the HS cases had a higher Q_c at an axial position of 50 mm to 120 mm than observed in the corresponding MS cases; and 3) the MS = 0.80 case had about the same CRZ flow rate as the MS = 0.65 case up to an axial position of 105 mm above the base of the combustion chamber.

TABLE 3. Flow Rates in the Central Recirculation Zone (CRZ)

Axial Position, mm	CRZ Flow Rate, lpm			
	MS =0.65	HS 0.65	MS 0.80	HS 0.80
10	35.8	74.5	48.7	99.1
20	37.4	73.8	58.2	105.1
30	31.7	72.8	40.0	139.1
40	30.5	83.2	41.9	162.2
60	73.6	182.0	66.1	340.1
80	84.9	281.5	139	353.6
100	311.3	515.0	119	1048.8
125	562.3	404.2	948.6	1013.4
150	808.2	488.2	1105.2	766.8
175	139.0	243.8	518.4	100.2

In Table 4, axial flow rates in the SRZ are reported at each of the axial positions where velocity data were taken. The flow rates through the SRZ were much greater and extended higher up into the combustion chamber for the MS cases than the HS cases. The flow rates were only calculated out to a radial position of about 40 mm to 45 mm. Some of the cases had a SRZ that extended beyond a radial position of 40 mm to 45 mm. For these cases, Q_s was integrated to the farthest radial position where data were taken. The flow rates that were not completely calculated to a zero axial velocity boundary were labeled with a (*) in Table 4. The values of Q_s had a greater magnitude than listed.

Even though a portion of the SRZ flow rates for the MS cases could not be calculated, the MS cases still had a greater Q_s than the HS cases. The MS = 0.80 case had the largest Q_s . The MS = 0.80 case was the only case that had the SRZ extend up into the visible flame zone. The MS = 0.65 case had the second largest SRZ flow rates which peaked at 367 lpm, the HS = 0.65 case had the third largest SRZ flow rates

which peaked at 196 lpm, and the HS $\phi = 0.80$ case had the smallest SRZ flow rates which peaked at 100 lpm.

TABLE 4. Flow Rates in the Side Recirculation Zone (SRZ)

Axial Position (mm)	SRZ Flow Rate, lpm			
	MS $\phi = 0.65$	HS $\phi = 0.65$	MS $\phi = 0.80$	HS $\phi = 0.80$
10	160.0 *	195.5	417.6 *	100.6
20	268.5 *	151.0	459.4 *	4.0
30	366.7 *	4.4	729.0 *	DNE
40	81.8	DNE	112.0 *	DNE
60	DNE	DNE	57.8	DNE

DNE: did not exist
 * The recirculation zone extended beyond data boundary

The HS cases had larger CRZ flow rates than the MS cases at axial positions of 10 mm to 110 mm. The ignition zone was located below an axial position of 50 mm and the lower half of the visible flame zone was located from 50 mm to 110 mm. Therefore, HS cases had a larger CRZ flow rate, recirculating hot gases down through the lower half of the visible flame zone and into the ignition zone than for the MS cases. In addition, the MS case did not have a change in the CRZ until after an axial position of 105 mm. This suggested that the CRZ played only a small role in stabilizing the MS case. Large increases in the CRZ flow rate appear to occur in the visible flame zone. These large increases in the CRZ flow rate could partly be due to an increase in temperature. Further studies need to be made to identify the relationship between recirculated flow rates and temperature.

The MS cases had much larger SRZ flow rates than the HS cases in spite of limitations in completely calculating the SRZ flow rates for the MS cases. The MS $\phi = 0.80$ case was the only case where the SRZ extended up into the visible flame zone. It appears that the MS cases needed to have more recirculated hot gases coming down into the ignition zone to stabilize the flame. These conclusions support observations made earlier. The fact that the CRZ flow rates in the ignition zone are highest for the HS cases correlates with the larger values of w_{cu} in this region. These both indicate stronger recirculation in the HS cases, making the flame more stable. The fact that the SRZ flow rates are highest for the MS cases correlates with the larger values of w_{su} . These also both indicate stronger recirculation in the MS cases for the SRZ. However, only the MS $\phi = 0.80$ case extended up into the visible flame zone and thus only the MS $\phi = 0.80$ case had improved stability from the stronger recirculation.

CONCLUSIONS

The general objective of this study was to gain insight into the flow structure of a turbulent, swirling, premixed natural gas/air combustor by obtaining specific *in situ* velocity and turbulence data over axial, tangential, and radial ranges. A combustion chamber that reproduces the characteristics found in a modern annular gas turbine combustor was used to investigate the characteristics of a premixed natural gas/air flame using LDA at four operating conditions (HS and MS at $\phi = 0.65$ and 0.80).

A wide variation in flame shapes was visually observed for different combinations of swirl number and fuel equivalence ratio. The variations in flame shapes are primarily a result of the effect of the swirl intensity and fuel equivalence ratio on the flow field, with the magnitude of the airflow rate being of secondary importance.

The LDA velocity measurements confirmed these observations. Operation at $\phi = 0.80$ produced the most stable flames with both HS and MS injectors. The flame with the HS injector was more coalesced and closer to the injector than with the MS injector. At $\phi = 0.65$, the flame was quite unstable for both swirl injectors. With the MS injector, the flame was observed to oscillate between two different flame structures, one that was more or less attached to the vortex funnel, and one that was lifted well above the vortex funnel. The MS case at $\phi = 0.65$ was at the very edge of the lean flammability limit, and would on occasion extinguish. The flame stabilization was strongly influenced by the central recirculation zone for the HS $\phi = 0.80$ case, and by the side recirculation zone for the MS $\phi = 0.65$ case.

Comparison of the mean and standard deviation images illustrated the nature of the average flame structure, and the stochastic nature of the flame structure. Maximum standard deviation velocities were occurring in the same region as their corresponding maximum velocities. Past studies have suggested that high standard deviation correlated with high turbulence. Therefore, high turbulence is occurring in regions where there is a maximum velocity. PDFs support the observation strong shear layers and interfaces between recirculation zones in the combustion chamber.

The HS cases had a more intense central recirculation zone (CRZ) than the MS cases, whereas the lower stability MS cases had a more intense side recirculation zone (SRZ) than the HS cases. There are two possible reasons for having a less stable flame at MS $\phi = 0.65$ case. These are: 1) the CRZ is not bringing down significant amounts of hot reacted or partially reacted gases; and 2) the SRZs are not reaching up into the flame zone. The MS configuration seemed to be more dependent upon a SRZ that reaches up into the flame zone in order to sustain the flame.

The HS cases had larger CRZ flow rates than the MS cases in the ignition zone and in the lower region of the visible flame zone. The CRZ flow rates had large increases in the visible flame zone for all four cases. The MS cases had much larger SRZ flow rates than the HS cases.

ACKNOWLEDGMENTS

This paper presents results from a study that was funded in part by a U.S. Department of Energy's (DOE) Advanced Turbine Systems (ATS) program and with additional support by the Brigham Young University (BYU) Advanced Combustion Engineering Research Center (ACERC). This study was part of a more comprehensive effort by the U.S. Department of Energy's (DOE) Advanced Turbine Systems (ATS) program to develop advanced high efficiency gas turbines that demonstrated low pollution emissions.

REFERENCES

- Hedman, P. O., Fletcher, T. H., Graham, S. G., Timothy, G. W., Flores, D. V., and Haslam, J. K., 2002, "Observations of Flame Behavior in a Laboratory-Scale Pre-mixed Natural Gas/Air Gas Turbine Combustor from PLIF Measurements of OH," Paper GT-2002-20052, ASME International Gas Turbine and Aeroengine Congress and Exposition, Amsterdam, The Netherlands.
- Hedman, P. O., Flores, D. V., and Fletcher, T. H., 2002, "Observations of Flame Behavior in a Laboratory-Scale Pre-mixed Natural Gas/Air Gas Turbine Combustor from CARS Measurements of Gas Temperature," Paper GT-2002-20054, ASME International Gas Turbine and

- Aeroengine Congress and Exposition, Amsterdam, The Netherlands.
3. Flores, D. V., 2002, Ph.D. Dissertation, In Progress, Chemical Engineering Department, Brigham Young University, Provo, Utah 84602.
 4. Cannon, S. M., B. S. Brewster, and L. D. Smoot, 1998, "Stochastic Modeling of CO and NO in Premixed Methane Combustion," *Combustion and Flame*, Vol. 113, pp. 135-146.
 5. Cannon, S. M., B. S. Brewster, and L. D. Smoot, 1999, "PDF Modeling of Lean Premixed Combustion Using In Situ Tabulated Chemistry," *Combustion and Flame*, Vol. 119, pp. 233-252.
 6. Mallampalli, H. P., T. H. Fletcher, and J. Y. Chen, 1998, Evaluation of CH₄/NO_x Reduced Mechanisms Used for Modeling Lean Premixed turbulent Combustion of Natural Gas," *ASME Journal of Engineering for Gas Turbines and Power*, Vol. 120, pp. 703-712.
 7. Meng, F. L., B. S. Brewster, and L. D. Smoot, 1997, "Comprehensive Model for Lean Premixed Combustion in Industrial Gas Turbines – Part II. Application," Spring 1997 Meeting of the Western States Section/The Combustion Institute, Sandia National Laboratories, Livermore, California.
 8. Sturgess, G. J., D. G. Sloan, A.L. Lesmerises, S. P. Heneghan, and D. R. Ballal, 1992, Design and Development of a Research Combustor for Lean Blowout Studies,' *ASME Journal of Engineering for Gas Turbines and Power*, Vol. 114, pp. 13-19.
 9. Hedman, P. O., G. J. Sturgess, D. L. Warren, L. P. Goss, and D. T. Shouse, 1995, "Observations of Flame Behavior from a Practical Fuel Injector Using Gaseous fuel in a Technology Combustor," *ASME Journal of Engineering for Gas Turbines and Power*, Vol. 117, pp. 441-452.
 10. Hedman, P. O., and D. L. Warren, 1995, "Turbulent Velocity and Temperature Measurements from a Gas-Fueled Technology Combustor with a Practical Fuel Injector," *Combustion and Flame*, Vol. 100, pp. 185-192.
 11. Warren, D.L., and P. O. Hedman, 1997, "Differential Mass and Energy Balances in the Flame Zone from a Practical Fuel Injector in a Technology Combustor," *ASME Journal of Engineering for Gas Turbines and Power*, Vol. 119, pp. 352-361.
 12. Schmidt, S. E., and Hedman, P. O., 1995,"CARS Temperature and LDA Velocity Measurements in a Turbulent, Swirling, Premixed Propane/Air Fueled Model Gas Turbine Combustor," Paper Number 95-GT-64, ASME International Gas Turbine and Aeroengine Congress and Exposition, Houston, Texas.
 13. Roquemore, W. M., 1992. Personal Communication, Wright Laboratory, Wright Patterson Air Force Base, Dayton, Ohio.
 14. Gupta, A. K., D. G. Lilley, and N. Syred, 1994, *Swirl Flows*, Abacus Press, Kent, United Kingdom.
 15. Murray, R. L., 1998, "Laser Doppler Anemometry Measurements in a Turbulent, Premixed, Natural Gas/Air Combustor," M. S. Thesis, Chemical Engineering Department, Brigham Young University, Provo, Utah
 16. Webb, B. W., and P. O. Hedman, 1982, "LDV Measurements in a Simulated Entrained-Flow Coal Reactor," *Proceedings of the Symposium on Engineering Applications of Laser Velocimetry*, Fall ASME National Meeting, Phoenix, Arizona.
 17. Jones, P.G., 1984, "Fluid Dynamics Measurements in a Simulated Entrained Flow Combustor," M.S. Thesis, Brigham Young University, Provo, Utah.
 18. Lindsay, J.D., Hedman, P.O., and Smith, P.J., 1986 "LDA Measurements in Simulated Gasifier Flows with Swirl," *Proceedings of International Symposium on Laser-Doppler Velocimetry*, Lisbon, Portugal.
 19. Laser Velocimetry Systems, 1990, TSI Inc. 500 Cardigan Rd., P.O. Box 64394, St. Paul, MN 55164.
 20. Find Software, 1996, TSI Inc., 500 Cardigan Rd., P.O. Box 64394, St. Paul, MN 55164.